AGU PUBLICATIONS

JGR

Journal of Geophysical Research: Space Physics

RESEARCH ARTICLE
10.1002/2014JA020198

Key Points:
- Transition between shear flow-driven waves by varying pi/LE
- A stressed, collisionless magnetized plasma can relax by wave emission
- Relaxation of boundary layers can lead to broadband electrostatic noise

Correspondence to:
A. M. DuBois,
adubois2@wisc.edu

Citation:
DuBois, A. M., E. Thomas Jr., W. E. Amatucci, and G. Ganguli (2014), Experimental characterization of broadband electrostatic noise due to plasma compression, *J. Geophys. Res. Space Physics*, *119*, 5624–5637, doi:10.1002/2014JA020198.

Received 16 MAY 2014
Accepted 2 JUL 2014
Accepted article online 5 JUL 2014
Published online 25 JUL 2014

Experimental characterization of broadband electrostatic noise due to plasma compression

Ami M. DuBois[1], Edward Thomas Jr.[1], William E. Amatucci[2], and Gurudas Ganguli[2]

[1]Department of Physics, Auburn University, Auburn, Alabama, USA, [2]Plasma Physics Division, Naval Research Laboratory, Washington, District of Columbia, USA

Abstract For a wide variety of laboratory and space plasma environments, theoretical predictions state that plasmas are unstable to inhomogeneous flows over a very broad frequency range. Such sheared flows are generated in the Earth's magnetosphere and intensify during active periods. Specifically, for a velocity shear oriented perpendicular to a uniform background magnetic field, the shear scale length (L_E) compared to the ion gyroradius (ρ_i) determines the character of the shear-driven instability that may prevail. An interpenetrating plasma configuration is used to create a transverse velocity shear profile in a magnetized plasma column, a condition similar to that found in the natural boundary layers. The continuous variation of ρ_i/L_E and the associated transition of the instability regimes driven by the shear flow mechanism are demonstrated in a single laboratory experiment. Broadband wave emission correlated to increasing/decreasing stress (i.e., ρ_i/L_E), a characteristic signature of a boundary layer crossing, is found under controlled and repeatable conditions. This result holds out the promise for understanding the cause and effect of the in situ observation of broadband electrostatic noise.

1. Introduction

In a previous letter [*DuBois et al.*, 2013b], it was shown that a compressed, magnetized plasma layer can give rise to broadband electrostatic noise (BEN) in a laboratory experiment. Depending on the level of compression (measured from the ratio of the ion gyroradius to the velocity shear scale length), wave emission from below the ion cyclotron frequency up to the lower hybrid frequency ($\omega_{\mathrm{LH}} = (\omega_{pi}\,\omega_{ce})/\sqrt{\omega_{pe}^2 + \omega_{ce}^2}$) was observed, where $\omega_{pi,e}$ is the ion, electron plasma frequency and $\omega_{ci,e}$ is the ion, electron cyclotron frequency. This paper presents a detailed experimental characterization of the BEN phenomena performed under a controlled and repeatable laboratory plasma environment.

The BEN signature has been observed in space plasmas for decades [*Gurnett and Frank*, 1977; *Eastman and Frank*, 1984; *Parks et al.*, 1984; *Cattell and Mozer*, 1986; *Lakhina*, 1987; *Kintner et al.*, 1996; *Andre et al.*, 2001], but the cause and effect of the phenomena are still debatable. It is found that BEN intensifies during active periods when the Earth's magnetosphere is compressed by external forces of solar origin. Thinning of the magnetotail due to compression is observed during these active periods [*Takahashi and Hones*, 1988]. Natural boundary layers, such as the magnetopause and the plasma sheet boundary layer (PSBL), are compressed, and consequently, strong sheared flows caused by highly localized ambipolar electric fields arise [*Romero et al.*, 1990; *Romero and Ganguli*, 1994] and are observed [*Cattell et al.*, 1982; *Orsini et al.*, 1984; *Jacquey et al.*, 1994]. The highly stratified nature of the magnetotail region is now well established [*Sarafopoulos et al.*, 1997] and cannot be ignored in theoretical models. In particular, the inhomogeneous electric fields, which are an integral part of the equilibrium state, significantly affect the dispersive properties of the medium and are essential to the origin of BEN [*Ganguli et al.*, 1994b]. As these boundary layers are compressed, the ratio of the ion gyroradius (ρ_i) to the shear scale length, L_E (a measure of how strong the shear magnitude is in the plasma), increases, and the observations of BEN have been widely reported [*Gurnett and Frank*, 1977; *Parks et al.*, 1984; *Cattell and Mozer*, 1986; *Lakhina*, 1987; *Kintner et al.*, 1996; *Andre et al.*, 2001]. The frequency range of BEN extends from below the ion cyclotron frequency up to the electron plasma frequency. Simulations performed by *Romero et al.* [1992] have confirmed that the free energy available in sheared flows in the compressed boundary layers can give rise to BEN spectra. Others [*Grabbe and Eastman*, 1984; *Matsumoto et al.*, 1994; *Omura et al.*, 1994] have analyzed the origin of BEN assuming an infinite homogeneous plasma equilibrium model with homogeneous beams, although the presence of beams is sometimes questionable [*Angelopoulos et al.*, 1993] and how the solutions are affected by the inhomogeneous electric field is not known.

Table 1. A Hierarchy of Microinstabilities That Can Be Triggered by Velocity Shear [*Ganguli et al*., 1994a, 2002]

Regime	Transverse Shear Flow	Parallel Shear Flow
$\rho_i > L_E$ $\omega \sim \omega_{LH}$	Electron-Ion Hybrid (EIH) Instability	Shear-Driven Lower Hybrid Instability
$\rho_i \sim L_E$ $\omega \sim \omega_{ci}$	Inhomogeneous Energy-Density-Driven (IEDD) Instability	Shear-Driven Ion Cyclotron Instability
$\rho_i < L_E$ $\omega < \omega_{ci}$	Kelvin-Helmholtz Instability	Shear-Modified Ion Acoustic and D'Angelo Instabilities

Kinetic theory described by *Ganguli et al*. [1988a, 1988b, 1994a, 1994b] states that plasmas are unstable to transverse and parallel inhomogeneous flows over a very broad frequency and wavelength range. The theoretical predictions discuss a hierarchy of distinct modes of oscillation [*Ganguli et al*., 1994a, 2002] (Table 1) that can exist in a plasma in the presence of a transverse and/or a parallel sheared flow. This hierarchy of instabilities, where the magnitude of the shear frequency compared to the ion cyclotron frequency (ω_s/ω_{ci}) determines the character of the mode that may prevail [*Ganguli et al*., 1994a], is likely to make up the BEN spectrum that is often observed by satellites because they are directly triggered by the magnitude of stress. Since ω_s is inversely proportional to the shear scale length, $\omega_s = dV_{E\times B}/dx \sim 1/L_E$, where $V_{E\times B}$ is the inhomogeneous cross-field flow, the instabilities may also be characterized by a shear scale length compared to the ion gyroradius. This ratio (ρ_i/L_E) acts as a surrogate for the magnitude of stress that a plasma layer is subjected to and can be exploited in laboratory experiments to model the varying degree of stress resulting in the transition between the modes.

The instabilities shown in Table 1 have each been studied separately in different experimental devices. Specifically for transverse sheared flows, the Kelvin-Helmholtz instability ($\rho_i < L_E$ and $\omega < \omega_{ci}$) has been studied in both Q-machines [*Kent et al*., 1969; *Jassby*, 1970, 1972] and in fusion experiments [*Cianciosa*, 2012]. In the regime where $\rho_i \sim L_E$, a different shear-driven instability arises in the plasma that has a frequency, $\omega \sim \omega_{ci}$. This instability mechanism is described as the inhomogeneous energy-density-driven (IEDD) instability [*Ganguli et al*., 1988b] and is distinct from the Kelvin-Helmholtz instability. Studies at West Virginia University [*Amatucci et al*., 1994; *Koepke et al*., 1994, 1998] have characterized the IEDD instability in the presence of a magnetic field-aligned current in a Q-machine. Experiments at the Naval Research Laboratory [*Amatucci et al*., 1996, 1998] and at Auburn University [*Thomas et al*., 2003; *Eadon*, 2011] studied the IEDD instability in linear magnetized plasma experiments with a virtually nonexistent field-aligned current. The electron-ion hybrid (EIH) instability ($\omega \sim \omega_{\mathrm{LH}}$) arises when ρ_i becomes much larger than L_E, leaving the ions effectively unmagnetized while the electrons remain magnetized in the shear layer. The EIH instability was experimentally characterized by *Matsubara and Tanikawa* [2000], by *Santhosh Kumar et al*. [2002], by *Amatucci et al*. [2003], and more recently by *DuBois* [2013] and *DuBois et al*. [2014]. All of these instabilities have a single free energy source, a transverse shear flow, but the physics of the energy extraction to support growth are different [*Ganguli et al*., 1988a; *Ganguli*, 1997].

The experiment presented in this paper is the first to show the continuous transition between modes and the interrelation between the various transverse shear-driven modes and BEN, which is the basis of the compression/relaxation process of plasma in boundary layers. The experimental results are separated into two parts. First, the demonstration of the continuous variation of the ratio ρ_i/L_E and the associated transition of the instability regimes in a single laboratory experiment is discussed. Second, each shear-driven mode is examined more closely, and it is shown that the characteristics of the three modes are consistent with those exhibited by known shear-driven modes such as the Kelvin-Helmholtz, the IEDD, and the EIH instabilities.

2. Experimental Setup

The experiment described in this paper was performed using the Auburn Linear Experiment for Instability Studies (ALEXIS) device [*Wallace et al*., 2004; *Eadon et al*., 2011; *DuBois et al*., 2013a], which is a 1.7 m long, 10 cm diameter magnetized cylindrical plasma column designed to study sheared plasma flows. The experiment is run in a steady state double-plasma configuration, which is based upon a design first reported by *Amatucci et al*. [2003] and is described in detail by *DuBois et al*. [2013a], so only a brief summary of the device is given here. ALEXIS has five main sections that make up the vacuum chamber, which can be seen in Figure 1: (A) the radio frequency (RF) antenna, (B) a standard six-way cross, (C) the main chamber, (D) a

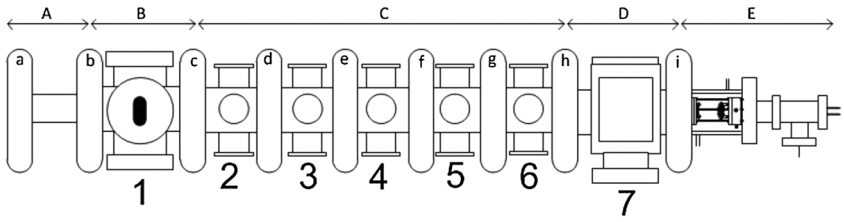

Figure 1. The Auburn Linear Experiment for Instability Studies (ALEXIS) has five main components: (A) the antenna, (B) a standard six-way cross, (C) the main chamber, (D) a custom box that can be used for optical access, and (E) a double-walled water-cooled section. The ports are numbered 1 (closest to the antenna) to 7 (farthest from the antenna). The magnets are lettered *a* through *i*.

custom box used for optical access, and (E) the double-walled, water-cooled section that houses a secondary plasma source. The ports are labeled using numbers 1 through 7, and the electromagnets, which produce a uniform axial magnetic field, are labeled *a* through *i*. Plasmas in ALEXIS are generated with argon neutral gas.

In its present configuration, ALEXIS uses two plasma sources—one at each end of the vacuum chamber. Primary plasmas in ALEXIS are generated using a 13.56 MHz, 600 W RF power supply. A matching network is used to couple the RF power from the antenna (section A in Figure 1) into the plasma. The secondary plasma source is located in the water-cooled section (section E in Figure 1) and is designed to have a much smaller diameter (2.5 cm) than the main RF-generated plasma (10 cm). The secondary source, which consists of three separate tungsten filaments connected in parallel, is a hot filament plasma source; i.e., it uses the thermionic emission of electrons from a heated wire to produce a plasma [*Nottingham*, 1936]. A blocking disk, located in port 1 in Figure 1, creates void region in the center of the primary RF plasma, which is then filled in by the smaller diameter filament plasma source, creating an interpenetrating, dual plasma configuration.

In order to perform the wave experiments, it is necessary to create a localized radial electric field at the boundary between the RF and filament plasmas to represent the compression phase during active periods [*Romero et al*., 1990; *Romero and Ganguli*, 1994]. It is possible to control this electric field in order to simulate increasing/decreasing stress by biasing a mesh placed 9 cm in front of the filament source to vary the plasma potential of the filament plasma. A high transparency mesh is placed directly in front of the RF antenna so that the RF plasma potential does not float to arbitrary potentials in order to ensure that a constant electric field between the plasmas can be reproduced. The biasing mesh is electrically connected to the blocking disk so that the entire filament plasma can be maintained at a single potential, which helps avoid drawing field-aligned current in the plasma. In the interpenetrating plasma configuration, variations in the radial direction are much stronger than in the axial direction, so the axial direction is nearly uniform for all practical purposes for the experiments discussed in this paper. A schematic of the interpenetrating plasma experiment is shown in Figure 2.

A range of in situ diagnostic probes were used in this experiment to measure plasma parameters and calculate radial profiles, including emissive probes (plasma potential and electric field) [*Eadon et al*., 2011], biased double probes (electron density and temperature) [*DuBois et al*., 2013a], and an electrically floating double tipped probe described here as a "*k*" probe (floating potential fluctuations and wave number) [*Eadon et al*., 2011; *DuBois*, 2013]. All of the probes are integrated into a data acquisition system and are controlled by a computer to move radially inward from $r = 5$ to $r = 0$ cm (corresponding to the cylindrical axis of the plasma), taking data every 0.2 cm to acquire radial profile of various plasma parameters.

3. Experimental Results

3.1. Continuous Variation of ρ_i/L_E

The goal of this study is to create a localized radial electric field and then vary the ion gyroradius with respect to the shear scale length by changing the magnetic field strength. This is done in order to model the important dynamic variability in the magnetotail during active periods and access the different resulting instability regimes defined by the magnitude of velocity shear. In this experiment, the magnetic field strength is varied from 90 to 590 G, while all other external experimental controls are held constant. The measured plasma parameters, such as the electron density and electric field, were observed to change spontaneously

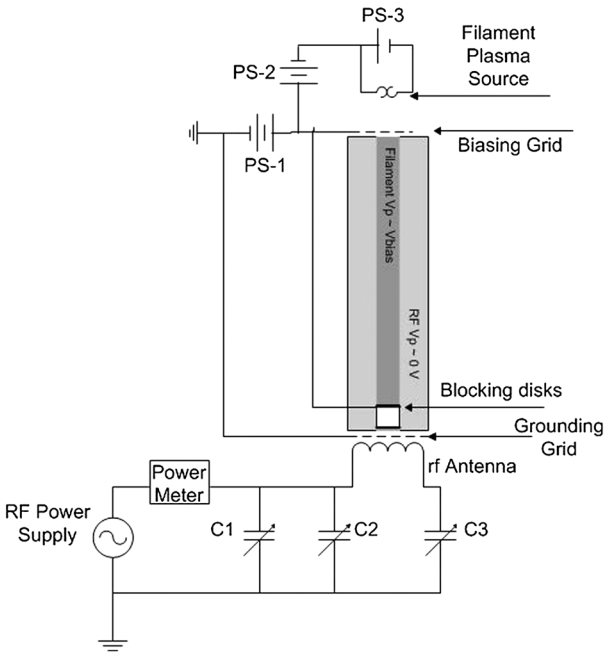

Figure 2. Schematic of the interpenetrating plasma experiment. The RF antenna and the matching network are shown at the bottom, and the hot filament circuit is shown at the top, where PS-1 controls the bias on the mesh, PS-2 controls the bias voltage on the filament source relative to the biasing mesh, and PS-3 resistively heats the filament source. The blocking disk is electrically connected to the biasing grid, which limits the amount of parallel current in the experiment.

as the magnetic field strength is varied. In this experiment, a small field-aligned current was measured on the face of the blocking disk and was observed to be nearly constant for all of the magnetic field strengths, as well as in the absence of the radial electric field. The axial drift velocity due to field-aligned (axial) current is considered to be negligible, because $V_{drift} \leq 0.1\, V_{the}$, where V_{the} is the electron thermal speed. Table 2 gives the baseline operating conditions for this experiment.

An electrically floating, heated emissive probe [*Eadon et al.*, 2011] located at port 2 (Figure 1) is used to measure the plasma potential as the probe is moved radially across the plasma column (Figure 3a). A radial electric field is then calculated from the plasma potential profile, and the shear scale length is calculated from the half width at half maximum of the radial electric field profile (Figure 3b).

Figure 4 shows the ρ_i (black circles) and the calculated L_E (pink squares) as a function of magnetic field strength. The measured scale length values range from 0.25 to 0.6 cm. The dashed horizontal line (pink) shows the average value of the shear scale length (0.4 ± 0.076 cm). The data shown in Figure 4 indicates that the three regimes defined by ρ_i/L_E, as described in Table 1, are accessible in the ALEXIS, interpenetrating plasma configuration. For magnetic field strengths less than 160 G (region 1, represented by the left vertical dashed line), the ion gyroradius is larger than the shear scale length, representing strong compression, and the shear-driven instabilities in the lower hybrid frequency range should be observed. For magnetic field strengths greater than 520 G (region 3, represented by the right vertical dashed line), the ion gyroradius is less than the shear scale length, representing weak compression, and the Kelvin-Helmholtz mode should be observable in the plasma. Between 160 and 520 G (region 2, between the vertical dashed lines), the ion gyroradius is comparable to the measured scale length, representing medium compression, and instabilities in the ion cyclotron frequency range should be observed in the plasma.

The response of the plasma was studied as the magnitude of the ratio ρ_i/L_E was varied from 0.55 to 3.39 (the average $L_E \sim 0.4$ cm is used). Frequency spectra are obtained from time-resolved Langmuir probe measurements of floating potential. The dashed vertical lines (red) in Figure 4 indicate the magnetic field strengths for which a transition in the mode frequency occurs. The logarithm of the mode frequency normalized to the ion cyclotron frequency is plotted as a function of ρ_i/L_E in Figure 5 to show the three distinct frequency modes observed in the plasma. For reference, under these operating conditions, the ion cyclotron frequency (i.e., $f_{ci} = \omega_{ci}/2\pi$) ranges from 3.6 kHz to 22.5 kHz as a function of increasing

Table 2. Experimental Operating Conditions

Parameter	Value
Neutral gas	Argon
Magnetic field	90 to 590 G
Neutral gas pressure	0.29 m torr
RF power	40 W
Filament emission current	60 mA
Filament bias	−20 V
Grid bias	80 V
Electron temperature	5 eV
Ion temperature	0.025 eV
Ion cyclotron frequency	3.6 to 22.5 kHz
Lower hybrid frequency	350 kHz

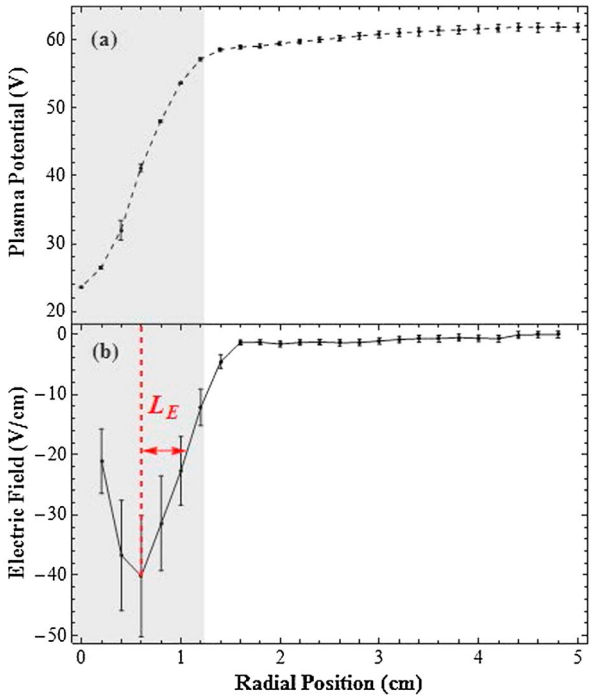

Figure 3. (a) The radial plasma potential measured using a hot emissive probe. (b) The radial electric field profile is calculated from the radial plasma potential profile, and the shear scale length, L_E, (red) is calculated as the half width at half maximum of the electric field profile.

magnetic field strength. The dashed lines (black) in Figure 5 indicate the ρ_i/L_E ratio where a transition in the wave frequency occurred. When ρ_i/L_E is between 0.55 and 0.62 (red data points corresponding to a high magnetic field strength), the mode frequency ($f \sim 1$ kHz) is much smaller than f_{ci} ($\omega/\omega_{ci} \sim 0.1 \pm 0.0035$), and when ρ_i/L_E is between 2.04 and 3.39 (green data points corresponding to a low magnetic field strength), the mode frequency ($f > 50$ kHz) is much higher than f_{ci} ($\omega/\omega_{ci} \sim 10.6 \pm 2.8$). When ρ_i/L_E is between 0.64 and 1.85 (blue data points), the mode frequency (13 kHz $< f <$ 15.2 kHz) is comparable to f_{ci} ($\omega/\omega_{ci} \sim 1.2 \pm 0.39$). Three distinct modes were observed in the plasma over a 5 order of magnitude spread in frequency (normalized by ω_{ci}) by varying ρ_i/L_E by only a factor of 7. This shows the sensitivity of the plasma compression (i.e., the magnitude of ρ_i/L_E) to the character of BEN.

Figure 6 shows a three-dimensional representation of the experimental measurements for each of the frequency ranges in the different ρ_i/L_E regimes. Each 3-D plot shows a spectrum of the fast Fourier transform (FFT) amplitudes (z axis), frequency (y axis), and the radial position (x axis). For the radial position axis, 0 cm denotes the center of the plasma column, and 5 cm corresponds to the edge of the vacuum vessel. In the x-z plane, the peak amplitude of the FFT spectrum is shown as a function of the radial position (radial wave amplitude profile). The FFT frequency spectrum is shown in the y-z plane. In the x-y plane, the frequency is shown as a function of the radial position. The plot color corresponds to the amplitude of the FFT spectrum, where red indicates a large amplitude and blue indicates a low amplitude. Dark blue indicates the noise floor.

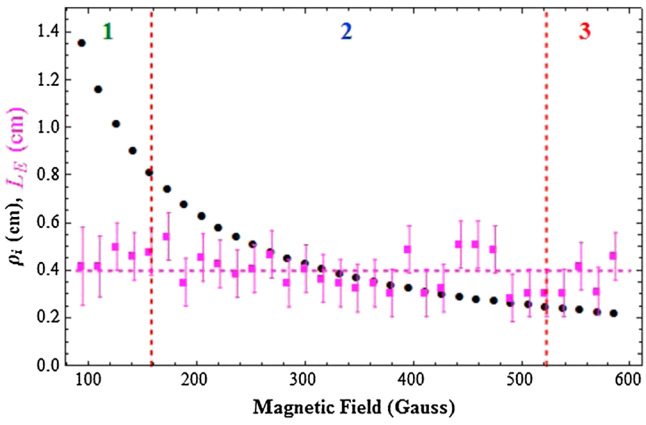

Figure 4. The ρ_i (black circles) and the measured L_E (pink squares) as a function of the magnetic field strength. The dashed horizontal line (pink) shows the average value of the measured shear scale length (0.4 ± 0.076 cm). The dashed vertical lines (red) indicate the magnetic field strengths where a transition in the ratio of ρ_i/L_E is observed, as well as a transition in the wave frequency. Region 1 (green) indicates the regime where $\rho_i \gg L_E$, region 2 (blue) is the regime where $\rho_i \sim L_E$, and region 3 (red) shows the data where $\rho_i < L_E$.

The first column in Figure 6 shows the 3-D plots for a low-frequency range between 0.3 and 10 kHz. The second column shows the three plots in the ion cyclotron frequency range (10 to 20 kHz), and the third column shows the plots for a high-frequency range between 30 and 100 kHz. Going down, a column represents increasing compression during active periods. It is important to note that the FFT spectrum amplitude scale in each column is different. The first column ranges from 1×10^{-4} AU to 5×10^{-3} AU. The amplitude range in the second column extends from

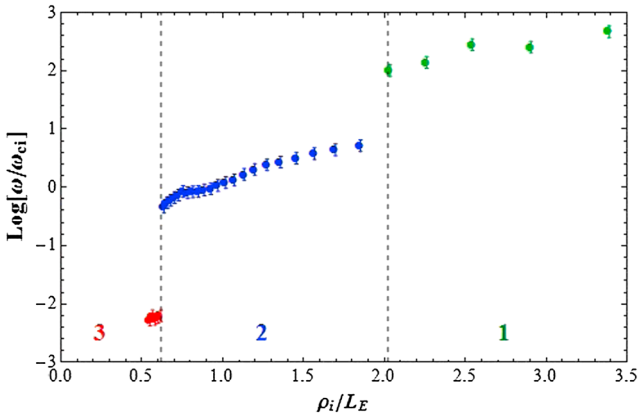

Figure 5. The log of ω/ω_{ci} is plotted as a function of the ratio of ρ_i/L_E. For a large ρ_i/L_E (low magnetic field strength), there is an instability with $\omega > \omega_{ci}$ (region 1, green). For a small ρ_i/L_E (large magnetic field), $\omega < \omega_{ci}$ (region 3, red). When $\rho_i \sim L_E$, the frequency is near ω_{ci} (region 2, blue). The dashed lines (black) indicate the ratio where a transition in the wave frequency occurs.

1×10^{-5} AU to 1×10^{-3} AU, and the amplitude in the third column ranges from 1×10^{-5} AU to 1×10^{-4} AU. Each row shows the 3-D plots for a different ρ_i/L_E regime, where the ratio of ρ_i/L_E increases going from the top row to the bottom row. For example, Figure 6a shows the 3-D plot for the low-frequency range when the ion gyroradius is smaller than the shear scale length, and Figure 6g shows the 3-D plot for the low-frequency range when the ion gyroradius is larger than the shear scale length. This figure shows that for each ρ_i/L_E regime, a wave exists in a limited frequency range. No other modes exist in the plasma at the same time and that only by changing the ratio of ρ_i/L_E is a new mode in a new frequency range accessible.

In the regime where $\rho_i < L_E$ ($\rho_i/L_E = 0.56$), there is a wave present below 10 kHz (Figure 6a), and at higher frequencies, there are no high-amplitude fluctuations present in the plasma (Figures 6b and 6c). When the ion gyroradius is comparable to the shear scale length ($\rho_i/L_E = 1.70$), Figure 6d shows that there is no longer a wave below 10 kHz, and Figure 6f shows that no wave exists above 30 kHz in the high-frequency range.

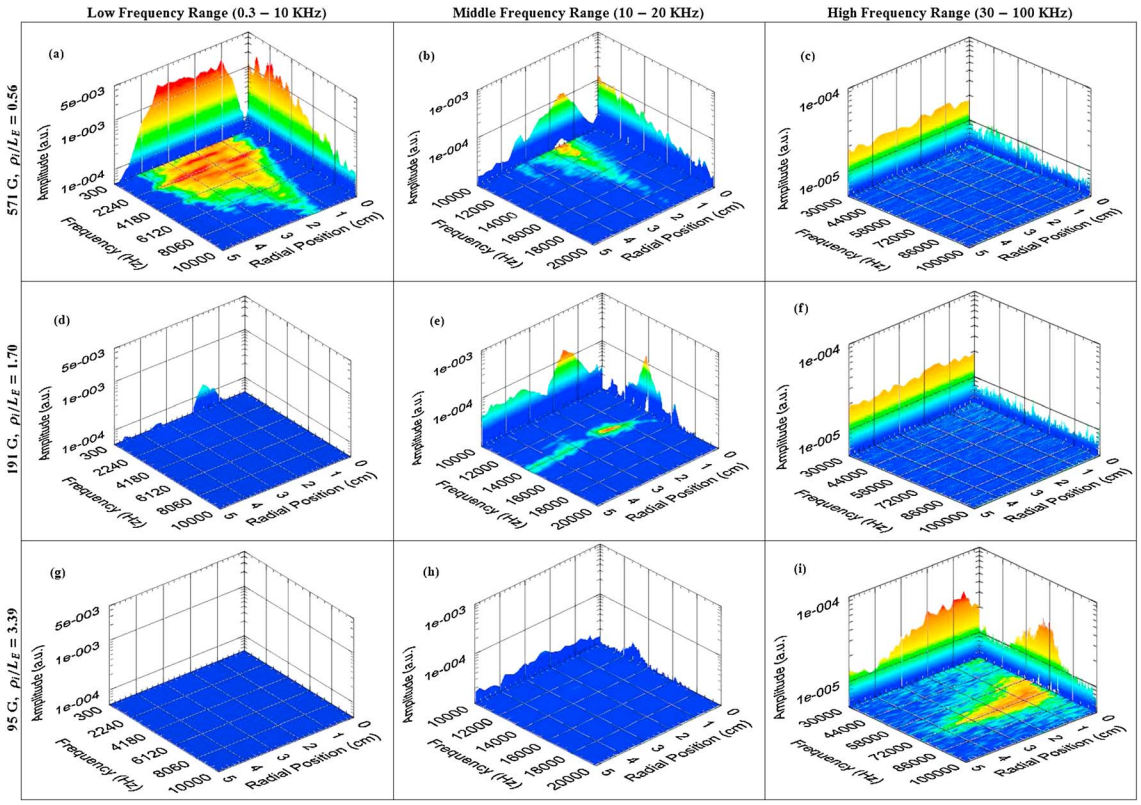

Figure 6. (first to third columns) The 3-D plots show the FFT amplitude on the vertical axis, frequency on the left axis, and radial position on the right axis. The plots show different frequency ranges going from left to right and show increasing values of ρ_i/L_E going from top to bottom. The color scale corresponds to the FFT amplitude where red indicates a high amplitude and dark blue represents the noise floor of the FFT spectrum.

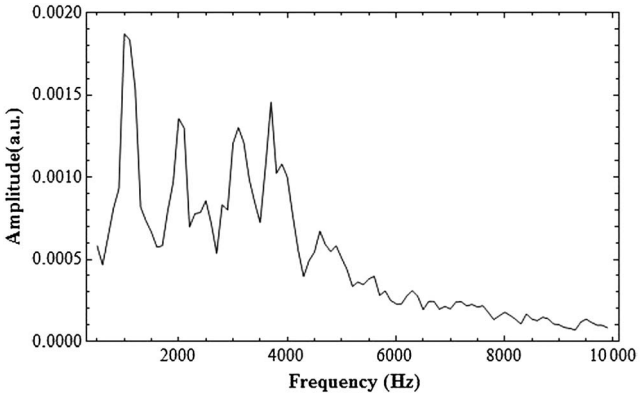

Figure 7. The Fourier spectrum when the ion gyroradius is less than the shear scale length (corresponding to a high magnetic field strength). The characteristic frequency is approximately 1 kHz, with three harmonics at higher frequencies. For this case, $\rho_i/L_E = 0.56$.

Figure 6e shows that a wave is now supported primarily in the middle-frequency range near the ion cyclotron frequency. Finally, in the last regime where the ion gyroradius is greater than the shear scale length ($\rho_i/L_E = 3.39$), no waves are excited at low frequencies, and the excited waves are observed near 70 kHz. Figure 6 shows that there are three distinct modes that are excited at various stages of compression.

3.2. Characterization of Shear-Driven Modes

To characterize the shear-driven modes observed in ALEXIS, the tips of a double Langmuir probe [*DuBois et al.*, 2013a] (located at port 4) are biased relative to each other to acquire a characteristic trace at different radial positions. The electron density and temperature are derived from the characteristic trace to calculate radial profiles. A "*k*" probe [*Eadon et al.*, 2011] (located at port 5) has two electrically floating tips with a separation distance (Δx) of 3 mm and is used to calculate the phase difference ($\Delta\varphi$) between two azimuthal or axial locations of a wave by measuring the floating potential fluctuations simultaneously on each probe tip. The amplitude and frequency of electrostatic waves in the plasma are calculated from the floating potential fluctuations at each radial position, and the wave number is calculated from the measured phase difference ($k = \Delta\varphi/\Delta x$) at the same position as the peak wave amplitude. In the next series of plots, the three distinct modes observed in the plasma are discussed.

3.2.1. Low-Frequency Range

The following plots correspond to the low-frequency shear-driven mode that arises when $\rho_i/L_E < 1$ (region 3 in Figure 4 and red data in Figure 5). Figure 7 shows the FFT spectrum of the low-frequency wave ($\rho_i/L_E = 0.56$) measured at the same radial position as the peak wave amplitude. The characteristic frequency is close to 1 kHz, with three harmonics near 2 kHz, 3 kHz, and 4 kHz. This spectrum is a very typical case of what is observed when the ion gyroradius is smaller than the shear scale length. The wave is located at a low frequency so that $\omega/\omega_{ci} = 0.11$.

Figure 8 shows (a) the wave amplitude profile, (b) the radial electric field profile, and (c) the radial electron density profile for the low-frequency wave. The wave amplitude profile shows that the wave extends over the entire plasma column, with a peak amplitude at $r = 1.6$ cm. There is a radially outward electric field with a peak value of 16 V/cm located at $r = 1.8$ cm. The electron density profile shows that the electron density peaks at $r = 2$ cm with a density of 5.5×10^{15} m^{-3}. Figure 8a shows that the wave packet is localized in the same region as the peak electric field (Figure 8b) and the peak electron density (Figure 8c). The electron density profile shows that there is a density gradient located in the plasma, with a peak density gradient at $r = 1.2$ cm. However, if the instability was driven by the density gradient instead of the electric field, the diamagnetic drift frequency (ω^*) would be much larger than the shear frequency (ω_s), and the mode observed in the plasma could be a drift wave. The ratio of the diamagnetic drift frequency to the shear frequency is $\omega^*/\omega_s = (k_y V_d)/(V_{E\times B}/L_E) \approx 0.047$, where V_d is the diamagnetic drift velocity. The density gradient is negligible compared to the electric field, ruling out the possibility that the low-frequency mode is a drift wave. In addition, drift waves are stabilized by velocity shear [*Gavrishchaka et al.*, 1996; *DuBois et al.*, 2012].

The parallel and perpendicular wave number components (relative to the background axial magnetic field) are measured to be $k_z = 8 \pm 6.7$ m^{-1} and $k_y = 138 \pm 23.4$ m^{-1}, respectively, with a ratio of $k_z/k_y = 0.058$ and a mode number ($m = k_y\, r$) of 2.2. The large perpendicular wave number compared to the small axial wave number indicated that the waves propagate primarily in the azimuthal direction. These signatures are consistent with the Kelvin-Helmholtz mode [*Romero and Ganguli*, 1993; *Hojo et al.*, 1995]. *Peñano et al.* [1998] showed that the growth rate for this wave is nonzero for mode numbers greater than 1 in a cylindrical device such as ALEXIS.

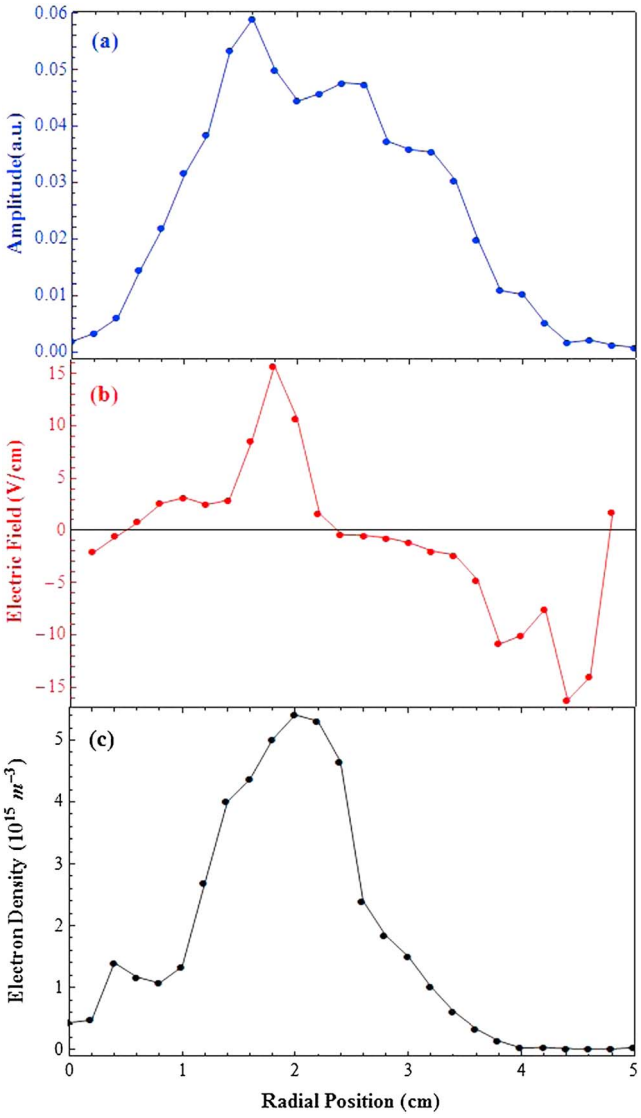

Figure 8. The (a) radial wave amplitude profile, (b) radial electric field profile, and (c) electron density profile for the low-frequency wave. For this case, $\rho_i/L_E = 0.56$.

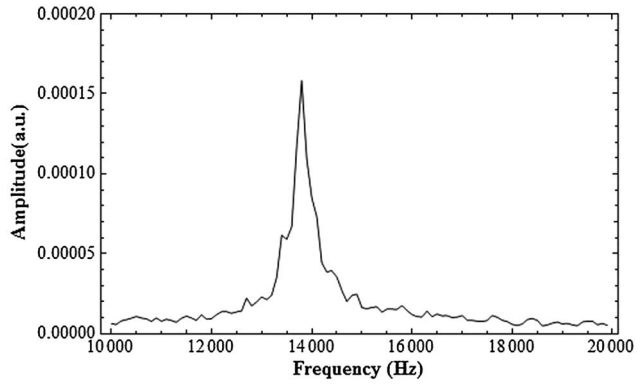

Figure 9. The Fourier spectrum for when the ion gyroradius is close to the shear scale length, $\rho_i/L_E = 1.7$.

3.2.2. Ion Cyclotron Frequency Range

The following plots correspond to the wave in the ion cyclotron frequency range when $\rho_i/L_E \sim 1$ (region 2 in Figure 4 and blue data in Figure 5). A typical spectrum for the waves found in this regime ($\rho_i/L_E = 1.70$) is shown in Figure 9. The spectrum in this case is highly localized in frequency space and shows that the wave has a much higher frequency ($\omega/\omega_{ci} = 1.9$) than in the previous case. This spectrum was measured at the same radial position as the peak wave amplitude.

Figure 10 shows the plasma parameter profiles, (a) the wave amplitude, (b) the radial electric field, and (c) the electron density, measured for the ion cyclotron-like mode. The wave amplitude profile shows that the wave is much more localized in space, with an amplitude peaking at $r = 1.6$ cm. A radially inward electric field, with a peak strength of 10.5 V/cm, is measured in the plasma (opposite in direction to the previous case). The electric field is now observed to peak near the center of the plasma column so that the peak wave amplitude occurs just outside the radial location of the peak electric field. The electron density is an order of magnitude less than in the previous case, peaking at 5×10^{14} m^{-3}. The electron density profile shows that the density in the filament plasma region is much less than that of the RF plasma, creating a density hole in the plasma. The wave amplitude peaks between the peak electric field and the peak electron density, with a mild density gradient compared to the electric field so that $\omega^*/\omega_s \approx 0.36$. The parallel and perpendicular components of the wave number are measured to be $k_z = 16 \pm 10.5$ m^{-1} and $k_y = 113 \pm 11.5$ m^{-1}, respectively, with a ratio of $k_z/k_y = 0.14$ (indicating that the waves propagate azimuthally) and a mode number of 2.2. These characteristics are indicative of the IEDD instability, which is driven by transverse velocity shear when the ion gyroradius is comparable to the shear scale length [*Ganguli et al.*, 1994a]. Analysis by *Peñano et al.* [1998] in

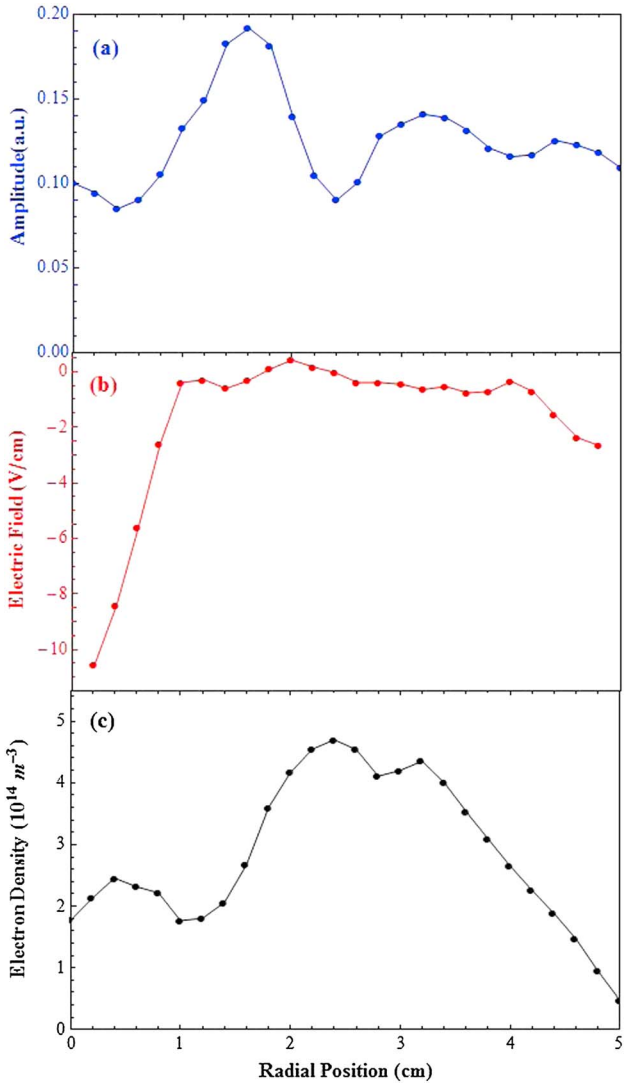

Figure 10. The (a) wave amplitude, (b) radial electric field, and (c) electron density profiles that correspond to the ion cyclotron-like wave. For this case, $\rho_i/L_E = 1.70$.

cylindrical geometry showed that the growth rate for the IEDD instability maximizes at $m = 1$. It is noted that in earlier studies of the IEDD instability in ALEXIS, it gave parameters of $k_z \sim 8\ m^{-1}$ and $k_y \sim 70\ m^{-1}$, or $k_z/k_y \sim 0.11$ with mode numbers between 1 and 2 [*Thomas et al.*, 2003]. Although using a very different configuration with different plasma sources and neutral gas, the axial and radial dimensions of ALEXIS remain the same as previous configurations. Therefore, it is reassuring that the wave packet for the current ALEXIS configuration is quite similar to past results.

The introduction of the radial electric field in the presence of a background magnetic field causes a Doppler shift in the wave frequency ($\omega_1 = \omega - k_y V_{E\times B}$) relative to the ion cyclotron frequency in the region over which the electric field is localized [*Ganguli et al.*, 1988b; *Koepke et al.*, 1994; *Thomas et al.*, 2003]. The energy density is negative in the electric field region due to the $E \times B$ drift. A nonlocal wave packet couples the positive and negative energy density regions together, causing a flow of energy out of the electric field region, which allows the IEDD instability to grow as long as $\omega_1 < 0$ [*Ganguli et al.*, 1988b]. The frequency of the IEDD instability in the lab frame (normalized to the ion cyclotron frequency), shown in Figure 11a, is observed to upshift from 0.71 ω_{ci} to 2.04 ω_{ci} as the electric field increases, which is expected for the nonresonant response of the IEDD instability, and was previously demonstrated at the Naval Research Laboratory by *Amatucci et al.* [1998]. Figure 11b shows the Doppler-shifted frequency of the wave (normalized to the ion cyclotron frequency) as is observed in the laboratory frame of reference. The Doppler-shifted frequency shown in Figure 11b varies from $-1.2\,\omega_{ci}$ to $-5.4\,\omega_{ci}$. The four points with electric field strengths greater than 8 V/cm are the last four data points before the transition to the higher-frequency mode occurs and corresponds to the ratios of ρ_i/L_E between 1.5 ($B = 206$ G) and 1.9 ($B = 175$ G), much higher than the rest of the data in the $\rho_i \sim L_E$ regime. The correlation between the increase in the Doppler-shifted frequency and the ρ_i/L_E regime change seems to indicate that these four data points may be a transitional mode which is a mixture between the IEDD instability and the observed lower hybrid mode.

3.2.3. Lower Hybrid Frequency Range

Finally, the next three plots correspond to the regime where $\rho_i/L_E > 1$ (region 1 in Figure 4 and green data in Figure 5). In this example, $\rho_i/L_E = 3.39$, and the wave frequency is much greater than the ion cyclotron frequency ($\omega/\omega_{ci} = 14.5$) but close to the lower hybrid frequency ($\omega/\omega_{LH} = 0.17$). The peak FFT amplitude was observed to increase with increasing electric field magnitude, with the mode frequency shifting from 55 kHz to 74 kHz. A typical frequency spectrum is shown in Figure 12, where the peak FFT amplitude occurs near 72 kHz.

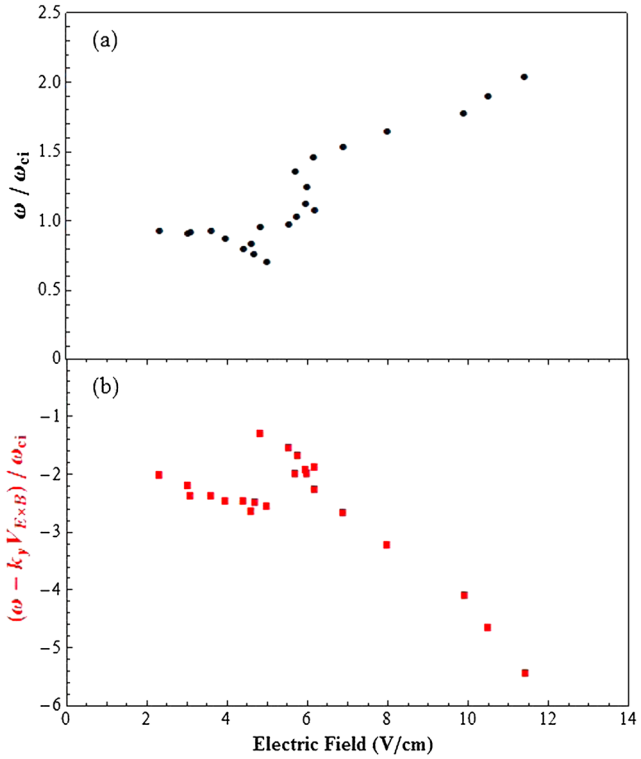

Figure 11. (a) The mode frequency normalized to the ion cyclotron frequency and (b) the Doppler-shifted frequency normalized to the ion cyclotron frequency plotted as a function of the electric field strength for the IEDD instability.

The data in Figure 13 show (a) the radial wave amplitude profile, (b) the radial electric field, and (c) the radial electron density profile. Figure 13a shows that the wave amplitude peaks at $r = 0.4$ cm and is localized near the boundary of the filament and RF plasmas, where the velocity shear is localized with a peak electric field of 40 V/cm that is oriented radially inward. The electron density is also observed to peak in the same region as the peak electric field, which creates a density gradient at the same radial location as the peak wave amplitude. A mild density gradient (with respect to the electric field gradient) was measured at $r = 0.6$ cm so that the ratio of the diamagnetic drift frequency to the shear frequency is $\omega^*/\omega_s \approx 0.06$. The measured perpendicular and parallel wave number components are $87 \pm 16.6\ m^{-1}$ and $10 \pm 17.4\ m^{-1}$, respectively, with a ratio of $k_z/k_y = 0.12$ (azimuthal propagation). The properties of the lower hybrid wave are consistent with the electron-ion hybrid (EIH) instability, although the observed frequency is somewhat lower than the lower hybrid frequency. Simulations by *Romero and Ganguli* [1993] showed that for the EIH mode, $k_z/k_y \sim 0.18$.

In order to explain the difference between the wave frequency and the lower hybrid frequency, experimental data were compared to the theoretical dispersion relation [*Ganguli et al*., 1988a; *DuBois*, 2013; *DuBois et al*., 2014]. Figure 14 shows the theoretical mode frequency (black solid line) and the growth rate (black dashed line) normalized to the lower hybrid frequency plotted as a function of the ratio of the shear scale length to the density gradient scale length (L_n). The theoretical model shows that when there is no (or weak) density gradient in the plasma (i.e., $L_E/L_n \ll 1$), the mode frequency is comparable to the lower hybrid frequency, which has been experimentally verified by *Amatucci et al*. [2003]. However, as the density gradient scale length decreases (L_E/L_n increases), the mode frequency decreases such that $\omega/\omega_{LH} < 1$ [*DuBois et al*., 2014]. The experimentally measured frequencies (red circles) and growth rates (blue squares) are plotted against the theoretically predicted values and show good agreement with the model, which indicates that the wave is the density gradient-modified EIH instability.

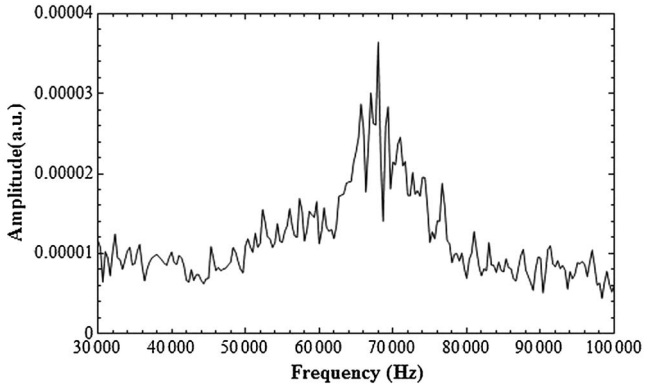

Figure 12. The frequency spectrum for the lower hybrid mode where the ion gyroradius is larger than the shear scale length so that $\rho_i/L_E = 3.39$.

4. Conclusion

The experiments discussed in this paper were performed in an interpenetrating, dual plasma configuration in the Auburn

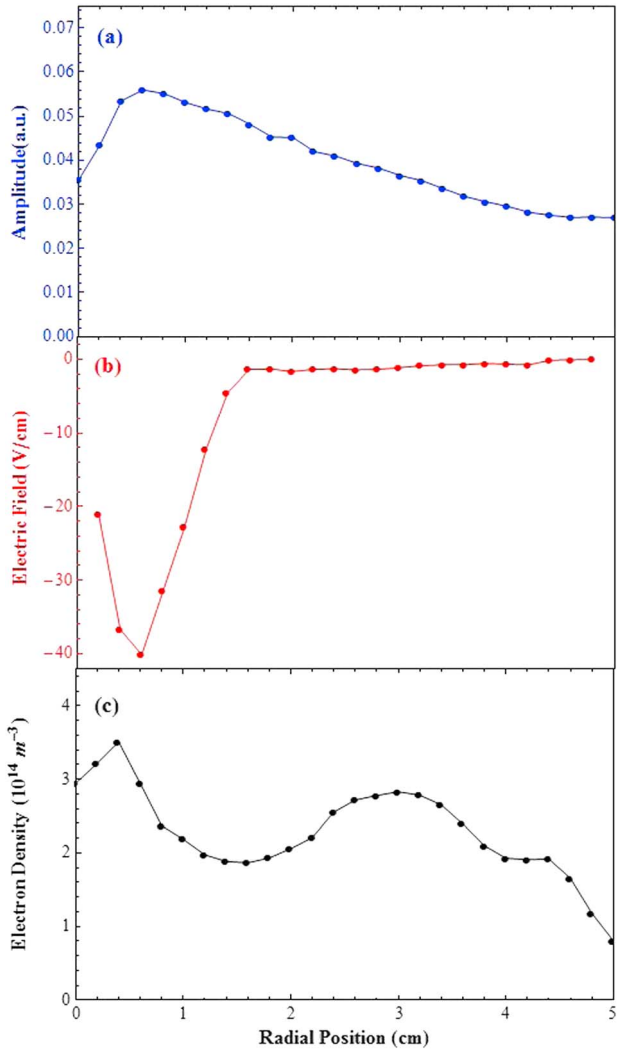

Figure 13. The (a) wave amplitude profile, (b) radial electric field profile, and (c) electron density profile for the lower hybrid mode where $\rho_i/L_E = 3.39$.

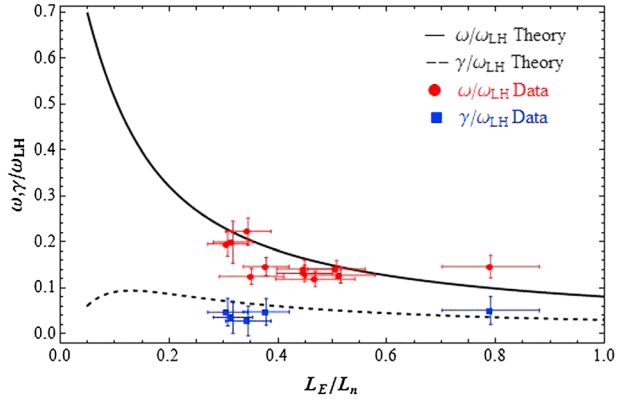

Figure 14. The theoretical curves for the frequency (solid line) and growth rate (dashed line) for the EIH instability are plotted as a function of the ratio of the shear scale length to the density gradient scale length (L_E/L_n). The experimentally measured frequencies (red circles) and growth rates (blue squares) are plotted against the theoretical model.

Linear Experiment for Instability Studies (ALEXIS). A strong $E \times B$ velocity shear was generated at the boundary between the two plasma columns by biasing the inner plasma source to different potentials relative to the outer, primary plasma source. The plasma compression/relaxation is modeled by varying the magnitude of ρ_i/L_E. This was achieved by varying the magnetic field strength to change the ion gyroradius, while all other external experimental parameters remained unchanged. At high magnetic field strengths, the ion gyroradius is less than the measured shear scale length ($\rho_i/L_E < 0.63$), and a low frequency wave ($\omega << \omega_{ci}$), identified as a Kelvin-Helmholtz instability, was observed in the plasma. As the ion gyroradius was increased by decreasing the magnetic field strength, the ratio of the ion gyroradius to the shear scale length was measured to be between 0.64 and 1.85, and a wave in the ion cyclotron frequency range identified as the IEDD instability arose in the plasma. At magnetic field strengths less than 160 G, the ratio of $\rho_i/L_E > 2$ and a lower hybrid wave was observed in the plasma such that $\omega \gg \omega_{ci}$. This shear-driven mode was characterized as the EIH instability, and it was shown that as a density gradient becomes more localized in the plasma, the mode frequency drops below the lower hybrid frequency [*DuBois et al.*, 2014]. Each of these modes has been studied individually in different laboratory devices and configurations, but the transition between the transverse shear-driven instabilities had never been observed in a single experiment under the continuous variation of the ratio of ρ_i/L_E.

In summary, we have reported the first experimental data, indicating that a stressed, collisionless magnetized plasma can relax by wave emission cascading through a broad frequency range [*DuBois et al.*, 2013b]. Three distinct modes spread over 5 orders of magnitude in frequency (normalized by ω_{ci}) arise when ρ_i/L_E is varied by a factor of 7. This is representative of the

compression/relaxation phase of the PSBL during disturbed conditions in the magnetosphere. In a small laboratory device like ALEXIS, it is difficult to access the ideal regimes for the different modes defined by $1 \ll \rho_i/L_E, \rho_i/L_E \sim O(1)$, and $\rho_i/L_E \ll 1$ while keeping other parameters nearly unchanged. But within the practical limitations, the transition between the hierarchy of transverse shear flow-driven modes and the consequent origin of BEN is quite clear in our experiment.

It is interesting that steepening of the low-frequency electrostatic [*Ganguli et al*., 1994a] or Alfvén waves [*Seyler et al*., 1998] in the ionosphere can generate localized regions of transverse electric field which can trigger the hierarchy of transverse shear-driven waves [*Peñano and Ganguli*, 1999]. These nonlinear electric field structures imply sheared transverse flows, similar to the boundary layers, and are found associated with the BEN signatures in the ionosphere [*Bonnell et al*., 1996; *Hamrin et al*., 2001]. The local dissipation of the BEN waves and the consequent plasma heating in the ionosphere represent the transport of energy from the distant magnetosphere through the Alfvén waves into the ionosphere.

The results of this work confirm the basic theory that plasma is unstable to localized transverse velocity shear in a very broad frequency range. These results also provide evidence for the theory described by *Ganguli et al*. [1994a, 1994b], which proposes that as a compressed boundary layer relaxes in a magnetized, collisionless plasma, it leads to a broadband noise signature that satellites have often observed while crossing magnetospheric boundary layers. In numerical simulations [*Romero et al*., 1990; *Romero and Ganguli*, 1993, 1994], the relaxation of a boundary layer is clearly visible as anticipated in theory, and they indicate that nonlinear evolution of these instabilities result in vortices, which may coalesce into larger vortices. However, given the space-time ambiguity of in situ observations, a significant component of the BEN spectrum may be attributable to the satellite's exposure to the variation of ρ_i/L_E while traversing through a boundary layer. Our experiment demonstrates that when the plasma is exposed to the variation of ρ_i/L_E, the spectral signature is different at different values of ρ_i/L_E, similar to the in situ observation. Thus, the experiment simulates a satellite traversal through the boundary layer and captures the tangible and observable effect of the compression/relaxation process. The results of this experiment are of particular interest to the space plasma community, where the plasma boundary layer dynamics play a major role in the transport and distribution of mass, energy, and momentum into different regions of geospace that affects near-Earth space weather.

Acknowledgments

This work is supported by grants from the Defense Threat Reduction Agency (HDTRA1-10-1-0019) and the Department of Energy—Office of Fusion Energy Sciences (DE-FG02-00ER54476). Work at NRL was supported by the NRL base funds. To request access to the data used for this paper, contact Ami DuBois (amd0012@auburn.edu).

Michael Liemohn thanks S. Singh and another reviewer for their assistance in reviewing this paper.

References

Amatucci, W. E., M. E. Koepke, J. J. Carroll, and T. E. Sheridan (1994), Observation of ion-cyclotron turbulence at small values of magnetic-field-aligned current, *Geophys. Res. Lett.*, *21*(15), 1595–1598, doi:10.1029/94GL00881.

Amatucci, W. E., D. N. Walker, G. Ganguli, J. A. Antoniades, D. Duncan, J. H. Bowles, V. Gavrishchaka, and M. E. Koepke (1996), Plasma response to strongly sheared flow, *Phys. Rev. Lett.*, *77*(10), 1978.

Amatucci, W. E., D. N. Walker, G. Ganguli, D. Duncan, J. A. Antoniades, J. H. Bowles, V. Gavrishchaka, and M. E. Koepke (1998), Velocity-shear-driven ion-cyclotron waves and associated transverse ion heating, *J. Geophys. Res.*, *103*(A6), 11,711–11,724, doi:10.1029/98JA00659.

Amatucci, W. E., G. Ganguli, D. N. Walker, G. Gatling, M. M. Balkey, and T. McCulloch (2003), Laboratory investigation of boundary layer processes due to strong spatial inhomogeneity, *Phys. Plasmas*, *10*(5), 1963, doi:10.1063/1.1562631.

Andre, M., R. Behlke, J. E. Wahlund, A. Vaivads, A. I. Eriksson, A. Tjulin, T. D. Carozzi, C. Cully, G. Gustafsson, and D. Sundkvist (2001), Multi-spacecraft observations of broadband waves near the lower hybrid frequency at the Earthward edge of the magnetosphere, *Ann. Geophys.*, *19*, 1471–1481.

Angelopoulos, V., C. F. Kennel, F. V. Coroniti, W. C. Feldman, J. T. Gosling, M. G. Kivelson, R. J. Walker, and C. T. Russell (1993), Observations of a quasi-static plasma sheet boundary, *Geophys. Res. Lett.*, *20*(24), 2813–2816, doi:10.1029/93GL01979.

Bonnell, J., P. M. Kintner, J. E. Wahlund, K. Lynch, and R. Arnoldy (1996), Interferometric determination of broadband ELF wave phase velocity within a region of transverse auroral ion acceleration, *Geophys. Res. Lett.*, *23*(23), 3297–3300, doi:10.1029/96GL03238.

Cattell, C. A., and F. S. Mozer (1986), Experimental determination of the dominant wave mode in the active near-earth magnetotail, *Geophys. Res. Lett.*, *13*(3), 221–224, doi:10.1029/GL013i003p00221.

Cattell, C. A., M. Kim, R. P. Lin, and F. S. Mozer (1982), Observations of large electric fields near the plasmasheet boundary by ISEE-1, *Geophys. Res. Lett.*, *9*(5), 539–542, doi:10.1029/GL009i005p00539.

Cianciosa, M. (2012), Measurements and modification of sheared flows and stability on the Compact Toroidal Hybrid stellarator, PhD dissertation, Auburn Univ., Auburn, Ala.

DuBois, A. M. (2013), Laboratory investigation of the dynamics of shear flows in a plasma boundary layer, PhD dissertation, Auburn Univ., Auburn, Ala.

DuBois, A. M., A. C. Eadon, and E. Thomas (2012), Suppression of drift waves in a linear magnetized plasma column, *Phys. Plasmas*, *19*(7), 072102, doi:10.1063/1.4731711.

DuBois, A. M., I. Arnold, E. Thomas, E. M. Tejero, and W. E. Amatucci (2013a), Electron-ion hybrid instability experiment upgrades to the Auburn Linear Experiment for Instability Studies, *Rev. Sci. Instrum.*, *84*(43503), 1–6, doi:10.1063/1.4799288.

DuBois, A. M., E. Thomas Jr., W. E. Amatucci, and G. Ganguli (2013b), Plasma response to a varying degree of stress, *Phys. Rev. Lett.*, *111*, (October 4), 145002, doi:10.1103/PhysRevLett.111.145002.

DuBois, A. M., E. Thomas, W. E. Amatucci, and G. Ganguli (2014), Density gradient effects on transverse shear driven lower hybrid waves, *Phys. Plasmas*, *21*(6), 062117, doi:10.1063/1.4886145.

Eadon, A. C. (2011), Modification of flow and flow driven instabilities in the Auburn Linear EXperiment for Instability Studies, PhD dissertation, Auburn Univ., Auburn, Ala.
Eadon, A. C., E. M. Tejero, A. M. DuBois, and E. Thomas (2011), Upgrades to the Auburn Linear EXperiment for Instability Studies, *Rev. Sci. Instrum.*, *82*, 063511, doi:10.1063/1.3594103.
Eastman, T. E., and L. A. Frank (1984), The Plasma Sheet Boundary Layer, *J. Geophys. Res.*, *89*(A3), 1553–1572, doi:10.1029/JA089iA03p01553.
Ganguli, G. (1997), Stability of an inhomogeneous transverse plasma flow, *Phys. Plasmas*, *4*(5), 1544.
Ganguli, G., Y. C. Lee, and P. J. Palmadesso (1988a), Electron-ion hybrid mode due to transverse velocity shear, *Phys. Fluids*, *31*(10), 2753.
Ganguli, G., Y. C. Lee, and P. J. Palmadesso (1988b), Kinetic theory for electrostatic waves due to transverse velocity shears, *Phys. Fluids*, *31*(4), 823, doi:10.1063/1.866818.
Ganguli, G., M. J. Keskinen, H. Romero, R. Heelis, T. Moore, and C. Pollock (1994a), Coupling of microprocesses and macroprocesses due to velocity shear: An application to the low-altitude ionosphere, *J. Geophys. Res.*, *99*(A5), 8873–8889, doi:10.1029/93JA03181.
Ganguli, G., H. Romero, and J. Fedder (1994b), Interaction between global MHO and kinetic processes in the magnetotail, in *Solar System Plasmas in Space and Time*, *Geophys. Monogr. Ser.*, vol. 84, edited by J. L. Burch and J. H. Waite, Jr., p. 135, AGU, Washington, D. C.
Ganguli, G., S. Slinker, V. Gavrishchaka, and W. Scales (2002), Low frequency oscillations in a plasma with spatially variable field-aligned flow, *Phys. Plasmas*, *9*(5), 2321–2329, doi:10.1063/1.1445181.
Gavrishchaka, V., M. E. Koepke, and G. Ganguli (1996), Dispersive properties of a magnetized plasma with a field-aligned drift and inhomogeneous transverse flow, *Phys. Plasmas*, *3*(8), 3091, doi:10.1063/1.871656.
Grabbe, C. L., and T. E. Eastman (1984), Generation of broadband electrostatic noise by ion beam instabilities in the magnetotail, *J. Geophys. Res.*, *89*(A6), 3865–3872, doi:10.1029/JA089iA06p03865.
Gurnett, D. A., and L. A. Frank (1977), A region of intense plasma wave turbulence on auroral field lines, *J. Geophys. Res.*, *82*(7), 1031–1050, doi:10.1029/JA082i007p01031.
Hamrin, M., M. Andre, G. Ganguli, V. V. Gavrishchaka, M. E. Koepke, M. W. Zintl, N. Ivchenko, T. Karlsson, and J. H. Clemmons (2001), Inhomogeneous transverse electric fields and wave generation in the auroral region: A statistical study, *J. Geophys. Res.*, *106*(A6), 10,803–10,816, doi:10.1029/2001JA900003.
Hojo, H., Y. Kishimoto, and J. W. Van Dam (1995), Stability criterion for Kelvin-Helmholtz mode in a cylindrical plasma, *J. Phys. Soc. Jpn.*, *64*(11), 4073–4076.
Jacquey, C., D. J. Williams, R. W. McEntire, A. T. Y. Lui, V. Angelopoulos, S. P. Christon, S. Kokubun, T. Yamamoto, G. D. Reeves, and R. D. Belian (1994), Tailward energetic ion streams observed at ~100 RE by Geotail-Epic associated with geomagnetic activity intensification, *Geophys. Res. Lett.*, *21*(25), 3015–3018, doi:10.1029/94GL01606.
Jassby, D. L. (1970), Evolution and large-electric-field suppression of the transverse Kelvin-Helmholtz instability, *Phys. Rev. Lett.*, *25*, 1567.
Jassby, D. L. (1972), Transverse velocity shear instabilities within a magnetically confined plasma, *Phys. Fluids*, *15*(9), 1590.
Kent, G. I., N. C. Jen, and F. F. Chen (1969), Transverse Kelvin-Helmholtz instability in a rotating plasma, *Phys. Fluids*, *12*(10), 2140, doi:10.1063/1.1692323.
Kintner, P. M., et al. (1996), The SCIFER experiment, *Geophys. Res. Lett.*, *23*(14), 1865–1868, doi:10.1029/96GL01260.
Koepke, M. E., W. E. Amatucci, J. J. Carroll, and T. E. Sheridan (1994), Experimental verification of the inhomogeneous energy-density driven instability, *Phys. Rev. Lett.*, *72*(21), 3355–3358.
Koepke, M. E., J. J. Carroll, and M. W. Zintl (1998), Excitation and propagation of electrostatic ion-cyclotron waves in plasma with structured transverse flow, *Phys. Plasmas*, *5*(5), 1671, doi:10.1063/1.872889.
Lakhina, C. S. (1987), Low-frequency electrostatic noise due to velocity shear instabilities in the regions of magnetospheric flow boundaries, *J. Geophys. Res.*, *92*(A11), 12,161–12,170, doi:10.1029/JA092iA11p12161.
Matsubara, A., and T. Tanikawa (2000), Anomalous cross-field transport of electrons driven by the electron-ion hybrid instability due to the velocity shear in a magnetized filamentary plasma, *Jpn. J. Appl. Phys.*, *39*, 4920–4932, doi:10.1143/JJAP.39.4920.
Matsumoto, H., H. Kojima, T. Miyatake, Y. Omura, M. Okada, I. Nagano, and M. Tsutsui (1994), Electrostatic solitary waves (ESW) in the magnetotail: BEN wave forms observed by GEOTAIL, *Geophys. Res. Lett.*, *21*(25), 2915–2918, doi:10.1029/94GL01284.
Nottingham, W. B. (1936), Thermionoic emission from tungsten and thoeriated tungsten filaments, *Phys. Rev. Lett.*, *49*, 78–97.
Omura, Y., H. Kojima, and H. Matsumoto (1994), Computer simulation of electrostatic solitary waves: A nonlinear model of broadband electrostatic noise, *Geophys. Res. Lett.*, *21*(25), 2923–2926, doi:10.1029/94GL01605.
Orsini, S., M. Candidi, V. Formisano, H. Balsiger, A. Ghielmetti, and K. W. Ogilvie (1984), The structure of the plasma sheet-lobe boundary in the Earth's magnetotail, *J. Geophys. Res.*, *89*(A3), 1573–1582, doi:10.1029/JA089iA03p01573.
Parks, G. K., et al. (1984), Particle and field characteristics of the high-latitude plasma sheet boundary layer, *J. Geophys. Res.*, *89*(A10), 8885–8906, doi:10.1029/JA089iA10p08885.
Peñano, J. R., and G. Ganguli (1999), Ionospheric source for low-frequency broadband electromagnetic signatures, *Phys. Rev. Lett.*, *83*(7), 1343–1346, doi:10.1103/PhysRevLett.83.1343.
Peñano, J. R., G. Ganguli, W. E. Amatucci, D. N. Walker, V. Gavrishchaka, and J. R. Peñano (1998), Velocity shear-driven instabilities in a rotating plasma layer, *Phys. Plasmas*, *5*(12), 4377, doi:10.1063/1.873175.
Romero, H., and G. Ganguli (1993), Nonlinear evolution of a strongly sheared cross-field plasma flow, *Phys. Fluids B*, *5*(9), 3163.
Romero, H., and G. Ganguli (1994), Relaxation of the stressed plasma sheet boundary layer, *Geophys. Res. Lett.*, *21*(8), 645–648, doi:10.1029/93GL03385.
Romero, H., G. Ganguli, P. J. Palmadesso, and P. B. Dusenbery (1990), Equilibrium structure of the plasma sheet boundary layer-lobe interface, *Geophys. Res. Lett.*, *17*(12), 2313–2316, doi:10.1029/GL017i013p02313.
Romero, H., G. Ganguli, and Y. C. Lee (1992), Ion acceleration and coherent structures generated by lower hybrid shear-driven instabilities, *Phys. Rev. Lett.*, *69*(24), 3503.
Santhosh Kumar, T. A., S. K. Mattoo, and R. Jha (2002), Plasma diffusion across inhomogeneous magnetic fields, *Phys. Plasmas*, *9*(7), 2946, doi:10.1063/1.1483074.
Sarafopoulos, D. V., E. T. Sarris, V. Angelopoulos, T. Yamamoto, and S. Kokubun (1997), Spatial structure of the plasma sheet boundary layer at distances greater than 180 RE as derived from energetic particle measurements on GEOTAIL, *Ann. Geophys.*, *15*, 1246–1256.
Seyler, C. E., A. E. Clark, and J. Bonnell (1998), Electrostatic broadband ELF wave emission by Alfven wave breaking, *J. Geophys. Res.*, *103*(A4), 7027–7041, doi:10.1029/97JA02297.

Takahashi, K., and E. W. Hones Jr. (1988), ISEE 1 and 2 observations of ion distributions at the plasma sheet-tail lobe boundary, *J. Geophys. Res.*, *93*(6), 8558–8582, doi:10.1029/JA093iA08p08558.

Thomas, E., J. D. Jackson, E. A. Wallace, and G. Ganguli (2003), Observations of low frequency oscillations due to transverse sheared flows, *Phys. Plasmas*, *10*(5), 1191, doi:10.1063/1.1567287.

Wallace, E. A., E. Thomas, A. C. Eadon, and J. D. Jackson (2004), Design and initial operation of the Auburn Linear Experiment for Instability Studies: A new plasma experiment for studying shear driven flows, *Rev. Sci. Instrum.*, *75*(12), 5160, doi:10.1063/1.1818491.